Hindawi
Journal of Chemistry
Volume 2019, Article ID 9325264, 9 pages
https://doi.org/10.1155/2019/9325264

Research Article

Photochemical Surface Modification of Titanium Dioxide Nanotube-Coated Surfaces by Ag-Hydroxyapatite Compositions

Khaled Rashwan[1], **Jevin Meyerink**[2], **Grigoriy Sereda**[1], **and Grant Crawford**[2]

[1]*Department of Chemistry, University of South Dakota, Vermillion, South Dakota, USA*
[2]*Department of Materials and Metallurgical Engineering, South Dakota School of Mines and Technology, Rapid City, South Dakota, USA*

Correspondence should be addressed to Khaled Rashwan; khaled.mahran@coyotes.usd.edu

Received 29 September 2018; Revised 29 November 2018; Accepted 5 December 2018; Published 15 January 2019

Academic Editor: Alessandro Volonterio

Silver-hydroxyapatite coatings prepared from Ag_3PO_4 microcrystals have been deposited on titanium dioxide nanotubes supported by titanium disks by photodecomposition of predeposited Ag_3PO_4 microcrystals or their coprecipitate with hydroxyapatite. The SEM-EDS characterization has confirmed excellent film uniformity and consistent deposition over the surface, which is essential for improving osseointegration of tunable antibacterial bone implants.

1. Introduction

As invaluable medical devices, titanium (Ti)-based orthopedic and dental implants have become standard as long-term bone replacements capable of supporting biogenic hydroxyapatite (HAp) structures [1, 2]. Despite their widespread application, early and late implant failures still occur as a result of (i) incomplete osseointegration, (ii) foreign body rejection, or (iii) the formation of pathogenic biofilms on the implant surface [3]. Ti and Ti alloys, commonly used in orthopedic and dental implants [4–6], are highly corrosion-resistant materials with impressive strength and a low density compared to stainless steels [7–9] A compact layer of naturally forming titanium dioxide (TiO_2), present on the titanium surface, has shown to enhance chemical bonding of growing bone tissue to the implant [2]. A significant research effort is aimed at enhancing bone growth to the Ti surface by tailoring surface roughness and chemical composition [10–12], including coating with HAp [13, 14] and other calcium phosphate ceramics [15]. HAp is a nanocomposite material with a mineral component similar in composition and structure to human bone tissue and has shown to have significant influence over cellular function when applied with specific nanotextures [16–22]. The idea of tailoring nanostructure of a material to influence the overall surface properties has gained major attraction [23, 24]. For instance, modification of a Ti surface with highly ordered TiO_2 nanotubes (NTs), fabricated via electrochemical anodization, has proven to be an effective method for influencing biological response mechanisms [25–27].

To this end, the literature is pervaded with coating methods designed to resolve a combination of the implant failure modes listed above by developing multifunctional implant modification procedures [2, 28–42]. While it is known that modifying the topography of the implant surface on the nanoscale has shown to be effective in terms of increasing osteogenic phenomena and lessening rejection [43], these coatings do not effectively prevent bacterial colonization. To combat unwanted bacterial growth, imbuing these coatings with antibacterial agents and hierarchical nanostructures, the materials' antibacterial properties are expected to increase dramatically.

Given that implant surfaces are at risk for infection throughout their lifetime, combating implant related infections via controlled, long-term delivery of an antibacterial agent to the local implant environment is critical. These preferred properties are often related to the structure and application technique of the antibacterial agent itself. Silver (Ag) is a known antibacterial agent usually deposited

on implants by photodecomposition of silver nitrate ($AgNO_3$) or deposition of preprepared Ag nanoparticles (NPs) [16, 44–46]. However, the resultant Ag coverage is often either nonuniform, likely associated with the low affinity of Ag to TiO_2, or requires the presence of additional agents (e.g., polyols) [47]. In addition, there is little control over the dynamics of Ag release from its deposits exposed to the implant-bone interface [16]. Therefore, a simple process is needed to evenly distribute Ag onto these nanostructured Ti surfaces while also offering a stable, long-term Ag release profile. Furthermore, studies have shown that a certain concentration of Ag^+ can have bactericidal capabilities while retaining cytocompatibility, which underscores the importance of controlled (both the quantity and location of Ag on the implant) deposition of Ag [16, 48]. The use of Ag for the treatment of infections in damaged tissue (e.g., wounds, ulcers, and burns) is common owing to the material's (i) antimicrobial properties against over 650 different pathogenic species [49], including antibiotic-resistant bacteria, (ii) chemical stability, and (iii) reduced risk for the development of bacterial resistance [16, 48, 50–53].

Here, we report deposition of silver-hydroxyapatite coatings on titanium dioxide nanotubes supported by titanium disks by phododecomposition of predeposited Ag_3PO_4 microcrystals or their coprecipitate with hydroxyapatite. First, a Ag_3PO_4-containing layer was introduced to the surface driven by the known affinity of Ag_3PO_4 to TiO_2 [54, 55]. Next, a uniform Ag coating on the implant's surface was produced by photodecomposition of Ag_3PO_4 particles which lead to the complete disappearance of the particulate. The capability of HAp to dissolve at high acidity levels creates a perfect opportunity for a controlled release of the antimicrobial silver when it is most needed, while the spatially controlled photodecomposition opens the door for depositing the patterns of antibacterial silver designed for a specific type of the bone implant.

2. Materials and Methods

2.1. Materials and Instrumentation. Silver nitrate ($AgNO_3$) was purchased from VWR. Nitric acid (HNO_3), sodium borohydride ($NaBH_4$), anhydrous sodium hydroxide (NaOH), sodium fluoride (NaF), anhydrous sodium phosphate dibasic (Na_2HPO_4), aqueous NH_3, sulfuric acid (H_2SO_4; 98.0 w/w.%), sodium fluoride (NaF; ≥99%), and ammonium fluoride (NH_4F) were purchased from Fisher Scientific, Pittsburgh, PA. Hydrogen peroxide polishing suspension was purchased from Fisher Scientific, Waltham, MA. Calcium nitrate [$Ca(NO_3)_2$] was purchased from Ward's National Science Establishment, Inc, Rochester, NY. Ammonium dihydrogen phosphate ($NH_4H_2PO_4$), citric acid, hydroxyapatite (HAp), and anhydrous ethylene glycol were purchased from Sigma Aldrich, St. Louis, MO. Colloidal silica and alumina powder was purchased from Pace Technologies, Tucson, AZ. Titanium (Ti) disks (99.7% pure, High-Strength Grade 5 Titanium) was purchased from McMaster-Carr, Elmhurst, IL. The pH meter (Omega PHB-212) was purchased from Omega Engineering, Stamford, CT. DC power supply (Mo #E3612A) from Agilent Technologies, Santa Clara, CA. The multimeter (Keithley 2100 Series: 6(1/2)-Digit USB Multimeter) was purchased from Tektronix, Beaverton, OR. Furnace was purchased from Thermolyne FB1415 m, Thermo Scientific, Waltham, MA. Imaging and elemental analysis experiments were conducted with a Sigma Zeiss Field Emission Scanning Electron Microscope (FE-SEM) and using an Oxford instruments X-Max^N 50 EDS probe. Transmission electron microscopy (TEM) micrographs were obtained using a Technai Spirit G2 Twin (FEI Company) TEM fitted with LaB6 filament operated at 120 kV. Samples were dispersed in water, then drop cast onto a carbon film (20–30 nm) on a 200 mesh copper grid (Electron Microscopy Sciences). Electron micrographs were obtained by projection onto an Orius SC200 CCD Digital Camera and recorded with Digital Micrograph software. A Newport 1000 W Xe arc lamp was used for photodecomposition experiments.

2.2. Nanostructured Ti Disks. Titanium dioxide nanotubes (TiO_2 NTs) were fabricated from titanium (Ti) substrates using a two-electrode electrolytic cell, comprised of Ti anode and platinum cathode. Ti disks with a thickness of 2.0 mm were cut from a 12.7 mm diameter Ti rod, then ground using progressively finer (i.e., 400, 600, 800, and 1200 grit) silicon carbide grinding paper, polished with 1.0 μm alumina powder and finished with a colloidal silica and hydrogen peroxide polishing suspension. Before anodization, disks were consecutively sonicated in deionized water and methanol for 5 mins each. TiO_2 NTs were fabricated using two different electrolytes, denoted as electrolyte 1 and electrolyte 2. Electrolyte 1 consisted of dissolved 0.2 M citric acid, 1 M H_2SO_4 (sulfuric acid 98.0 w/w.%), and 0.1 M NaF (sodium fluoride ≥ 99%) in continuously mixed deionized water. Electrolyte pH was adjusted to pH 3.5 through addition of anhydrous NaOH (sodium hydroxide) and measured using a pH meter. Electrolyte 2 was made by dissolving 0.3 wt.% NH_4F (ammonium fluoride ≥99%) and 2 vol.% H_2O in anhydrous ethylene glycol (EG). Electrolyte 1 was used to fabricate those specimens shown in Figures 1 and 2. All other results were generated using NTs fabricated using Electrolyte 2. It should be noted that the results of this study are not affected by the different electrolytes used and the purpose of this study was not to evaluate the influence of electrolyte composition on Ag deposition. Anodization was carried out using a constant applied potential of 20 V applied using a DC power supply with constant current recording carried out via using KI-Tool software (Tektronix, Beaverton, OR) and multimeter (Keithley 2100 Series: 6(1/2)-Digit USB Multimeter, Tektronix, Beaverton, OR). Anodization continued for 1 h with continuous electrolyte circulation. Following anodization, samples were sonicated in methanol for 3 mins and subsequently annealed for 1 h at 450°C.

2.3. Deposition of Ag on TiO_2 NTs via Photolysis of Ag Precursors

2.3.1. Ag Deposition on TiO_2 NT Disk by Photolysis of $AgNO_3$ (Control). A TiO_2 NT disk was treated with 4 mL of 2 M $AgNO_3$ for 15 mins with shaking, followed by rinsing with DI water (3 × 5 mL), and dried in air at 100°C for 13 min. The TiO_2 NT disk was irradiated with a Xe lamp for 8 min. The treated disks were characterized using SEM and EDS.

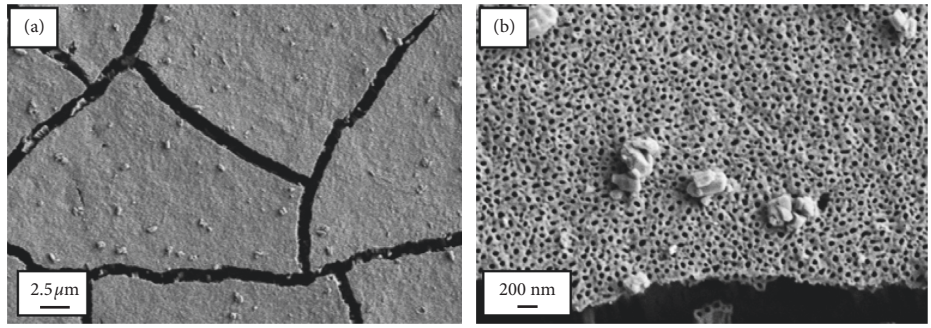

Figure 1: SEM micrographs of TiO_2 NT disks mixed with HAp solution and rinsed in water at (a) low and (b) high magnification.

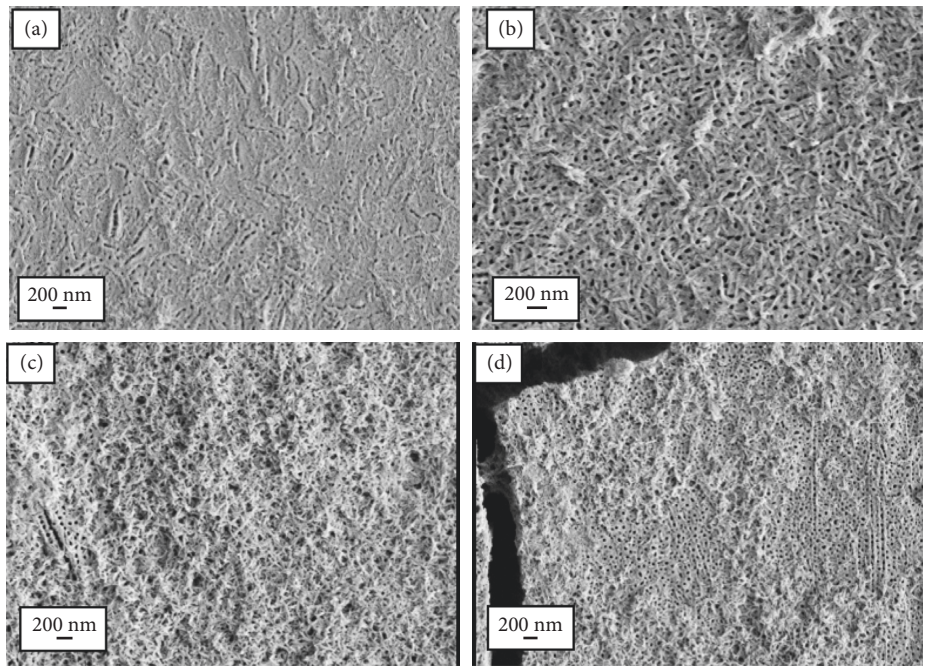

Figure 2: The NT disk surface following immersion in a suspension of HAp. The NT disk surface following precipitation of (a, b) HAp and (c, d) Ag-doped HAp layer at two respective magnifications.

2.3.2. Ag_3PO_4 Particle Deposition and Subsequent Photolysis. Another experiment was performed, where precipitation of Ag_3PO_4 onto the TiO_2 NT disks surface was achieved using known procedure [55]. Following the placement of an untreated TiO_2 NT disk into a beaker filled with 50 mL of water, 2.9 mL of 0.5 M $AgNO_3$ was added. This solution was slowly agitated at r.t. on a flat-head vortex mixer for 15 mins. Next, 50 μL of 0.1 M Na_2HPO_4 was added. The NT disk and the supernatant solution were agitated for 30 mins. The NT disk was washed with nanopure water for 1 min and kept at 70°C overnight. The coated disk was characterized using SEM and EDS and then exposed to UV irradiation for 15 mins with a Xe lamp. UV-treated Ag_3PO_4 NT disks were characterized using SEM and EDS.

2.4. Codeposition of HAp and Ag

2.4.1. Dip-Coating of HAp onto a TiO_2 NT Disk. An untreated TiO_2 NT disk was immersed in an aqueous 15 mL suspension of $3.31 * 10^{-2}$ mM HAp for 1 hr, rinsed, washed in water for 15 mins, and dried at 70°C overnight. The sample was characterized with SEM and EDS.

2.4.2. Sonosynthetic Precipitation of HAp onto a TiO_2 NT Disk. On another untreated TiO_2 NT disks, HAp was precipitated according to a modified known procedure [56]. Briefly, a TiO_2 NT disk placed into 25 mL of a 0.1 M calcium precursor solution (4.103 g $Ca(NO_3)_2$, 31.25 mL 29% NH_4OH in 250 mL of solution) was ultrasonicated on high power at 25°C. During ultrasonication, 25 mL of 0.06 M phosphate precursor solution (1.725 g $NH_4H_2PO_4$, 15.63 mL 29% NH_4OH in 250 mL of solution) was added at an approximate rate of 13 mL/min. The suspension was ultrasonicated for 1 min after the addition and left to age at r.t. undisturbed for 6 h. Next, the supernatant solution was decanted, and the residue was washed with 25 mL of water. The TiO_2 NT disk was removed from the beaker, rinsed, washed in water for 15 min, dried at 70°C overnight. A sample of the residue was added on a TEM grid for SEM, EDS, and TEM characterization.

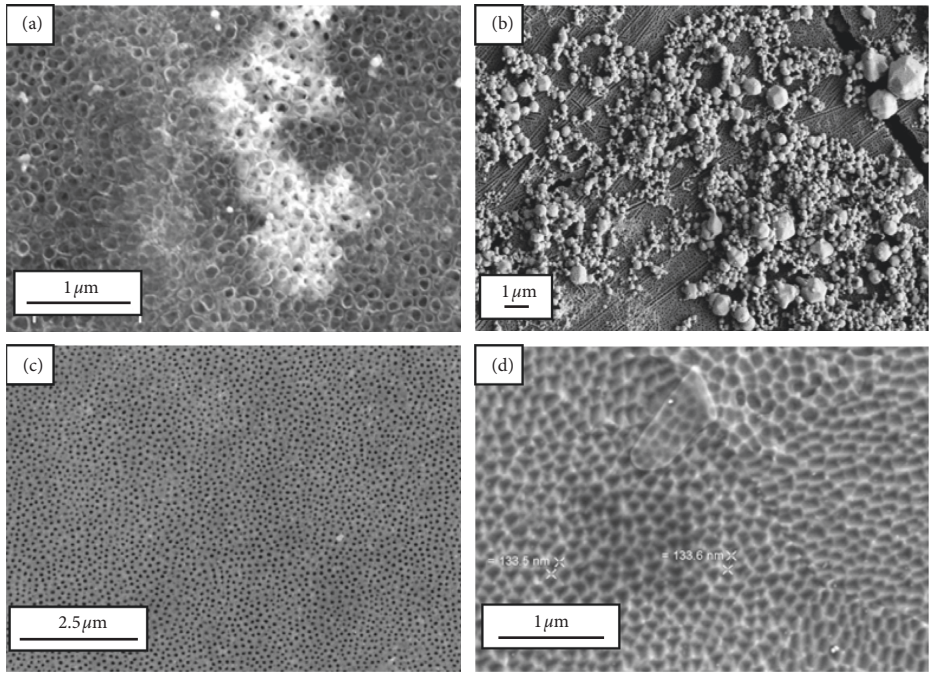

Figure 3: SEM micrographs of TiO_2 NT disks (a) treated with $AgNO_3$, followed by irradiation using Xe lamp, (b) Ag_3PO_4 crystals grown on the surface prior to irradiation, and (c, d) two different magnification of TiO_2 NT disks treated with Ag_3PO_4 followed by irradiation using Xe lamp.

Table 1: Elemental composition of the surface of the TiO_2 NT disks before and after $AgNO_3$ treatment, after growing Ag_3PO_4 microcrystals, and after photolysis of Ag_3PO_4 microcrystals obtained using EDS.

Element	Untreated (wt.%)	After $AgNO_3$ treatment (wt.%)	After growing Ag_3PO_4 microcrystals (wt.%)	After photolysis of Ag_3PO_4 microcrystals (wt.%)
Ti	59.4	45.5	24.0	27.0
O	36.1	45.1	64.6	72.1
Ag	—	1.1	2.2	0.6
C	4.5	5.2	8.5	<0.1
P	—	—	0.7	0.2

2.4.3. Coprecipitation of Ag_3PO_4 and HAp onto a TiO_2 NT Disk. This procedure was performed in a similar manner to the experimental procedures in Section 2.4.2, except for a further step by adding 1.7 g of $AgNO_3$ to the calcium precursor solution (1.651 g $Ca(NO_3)_2$, 1.7 g $AgNO_3$, 12.5 mL 29% NH_4OH in 100 mL of solution). The rest of the experiment was performed the same way. The remaining slurry in the beaker was collected and centrifuged for 8 mins at 3500 rpm. The remaining precipitate after decanting of the supernatant solution was dried in the oven overnight at 70°C, powdered in a mortar, and characterized as specified in Section 2.4.2.

3. Results and Discussion

3.1. Deposition of Ag on TiO_2 NTs via Photolysis of Ag Precursors

3.1.1. Ag Deposition on TiO_2 NT Disk by Photolysis of $AgNO_3$. In a control experiment, Ag was deposited by the known procedure of $AgNO_3$ photolysis [55], and produced a rather patchy (white area) deposition of the TiO_2 NT disk (Figure 3(a)). The EDS results, provided in Table 1, show the presence of Ag element at 1.1 wt.%.

3.1.2. Ag_3PO_4 Particle Deposition and Subsequent Photolysis. The Ag_3PO_4 nano- and microcrystals grown on a TiO_2 NT disk (Figure 3(b)) were retained by the TiO_2 NT surface even after rinsing with water due to the expected affinity of PO_4^{3-} to the TiO_2 surface. As illustrated in Figure 3(b), the procedure led to a wide particle size distribution. EDS results provided in Table 1, show the presence of Ag (2.2 wt.%) and P (0.7 wt.%). The oxygen content observed is higher than that for the usual untreated TiO_2 NT disks due to the oxygen of the Ag_3PO_4 microcrystals.

According to the SEM images provided in Figures 3(c) and 3(d), exposure of the treated surface to UV radiation led to complete breakdown of the Ag_3PO_4 particles. The EDS results provided in Table 1 illustrates the presence of 0.6 wt.% of Ag and 0.2% of P on the NT disk surface. The ratio of 3 : 1 Ag to *P* is maintained similar to the pre-irradiation ratio. This observation suggests a complete photodecomposition of the Ag_3PO_4 particles to a sub-nanometer layer of Ag. The elemental map presented in Figures 4(c) and 4(d) supports the observation, where Ag was evenly distributed along the surface, as was P after the irradiation of Ag_3PO_4 microcrystals.

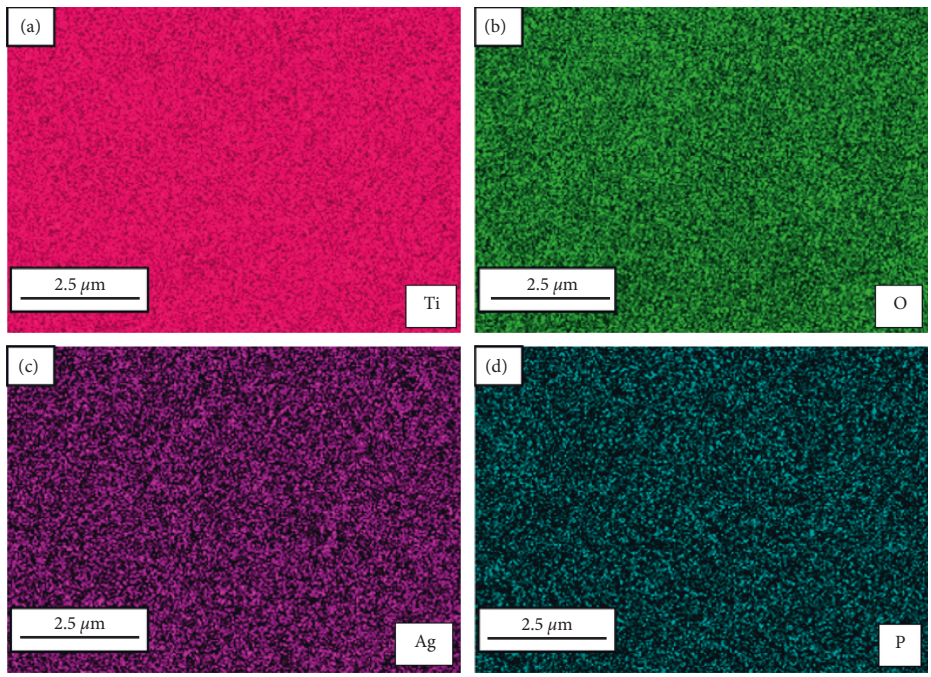

Figure 4: EDS elemental maps of TiO_2 NT disk treated with Ag_3PO_4 followed by irradiation using Xe lamp. The elements represent (a) titanium, (b) oxygen, (c) silver, and (d) phosphorus.

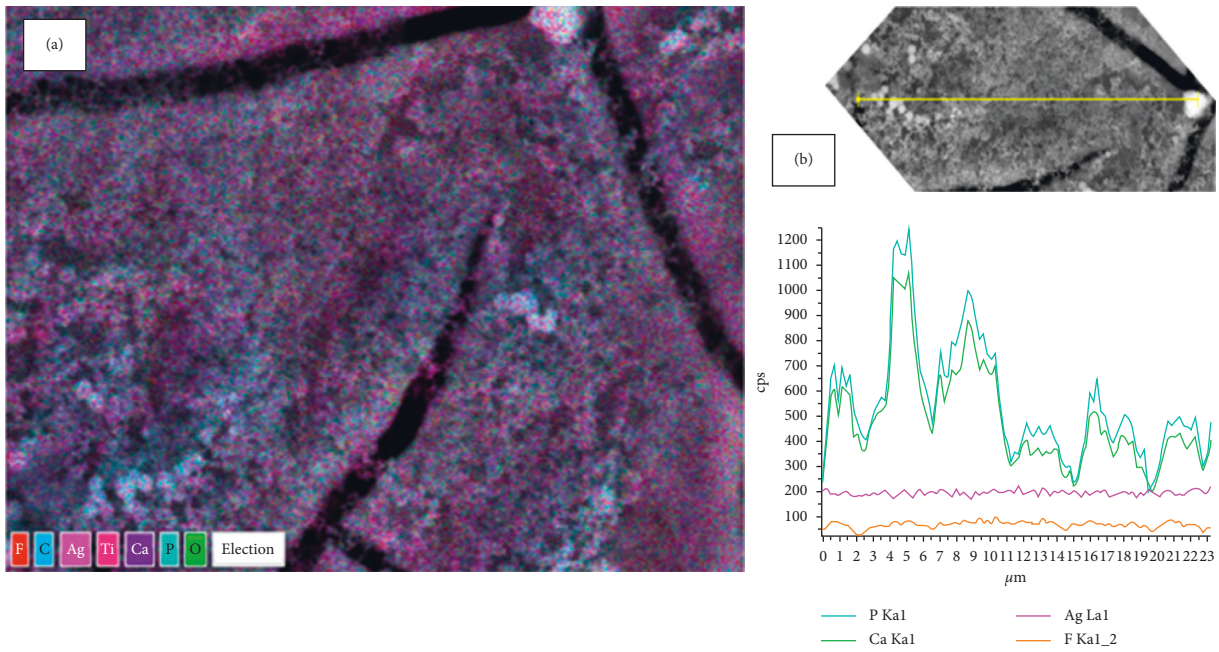

Figure 5: (a) Top-down SEM image and overlaid EDS elemental map and (b) EDS line scan obtained from the same region as (a) for coprecipitated Ag and HAp on TiO_2 NT disks.

Table 2: Elemental weight percentage of surface materials on the TiO_2 NT disks after deposition of Ag-doped HAp obtained using mapping and line scan EDS.

Element	Layered EDS mapping (wt.%)	Line scan EDS (wt.%)
O	70.8	70.0
Ti	22.2	22.4
C	3.5	3.0
Ca	1.9	2.1
P	1.3	1.4
Ag	0.3	0.3

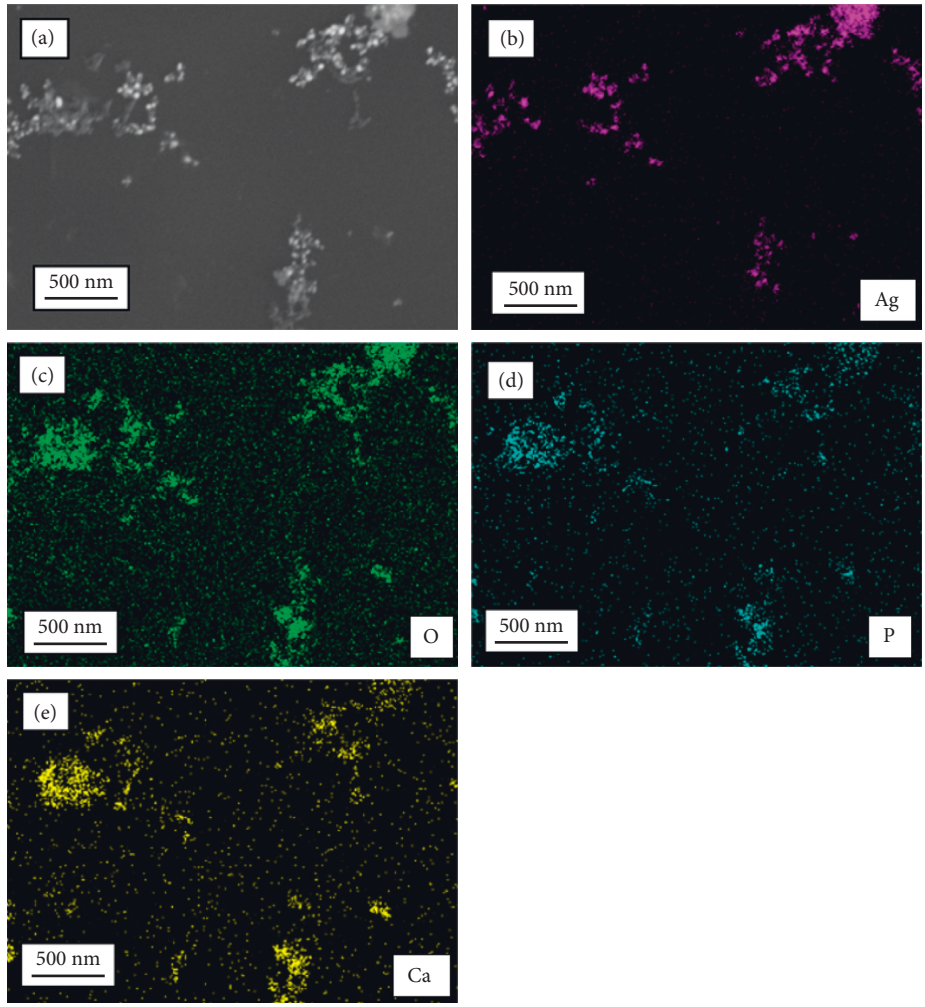

Figure 6: (a) SEM image of a TEM grid containing the coprecipitated Ag and HAp. EDS elemental maps: (b) Ag, (c) O, (d) P, and (e) Ca of the Ag-HAp NPs.

3.2. Codeposition of HAp and Ag

3.2.1. Dip-Coating of HAp onto a TiO_2 NT Disk (Control). The SEM images (Figures 1(a) and 1(b)) demonstrate the low affinity of the TiO_2 NT disk toward HAp after its immersion in the HAp aqueous suspension followed by rinsing with water in a control experiment.

3.2.2. Sonosynthetic Precipitation of HAp onto a TiO_2 NT Disk. The phosphate ions produced after the reaction (Formula (1)) may provide an opportunity to further deposit HAp on a Ag-coated implant:

$$4Ag_3PO_4 + h\nu \longrightarrow 3O_2 + 12Ag + 2P_2O_5 \quad (1)$$

Formula (1) is the expected reaction of Ag_3PO_4 photodecomposition. The h and ν represent Planck constant and the photon energy frequency, respectively.

Due to a lower surface concentration of Ag and sensitivity of the HAp-based coatings to external stimuli, coprecipitation of HAp with Ag^+ would provide more control over the release of Ag from the modified implant surface [57]. HAp crystals start to dissolve at pH less than 6, which would induce enhanced release of Ag in response to a bacterial infection, which is known to create an acidic microenvironment (pH ≤ 5) [58].

3.2.3. Coprecipitation of Ag_3PO_4 and HAp onto a TiO_2 NT Disk. To improve the deposition of HAp, HAp crystals were grown on the TiO_2 NT disks using ultrasonication, both with and without the addition of $AgNO_3$ (which produces Ag_3PO_4 resulted from mixing aqueous solutions of $AgNO_3$, $Ca(NO_3)_2$ and $NH_4H_2PO_4$). Growing HAp particles on the TiO_2 NT disk using ultrasonication led to the development of a porous array of rod-like HAp crystals (Figures 2(a) and 2(b)). In addition, the HAp surface coverage was significantly improved compared to simple immersion treatment (Section 3.2.1). The affinity remained high when HAp was coprecipitated with Ag_3PO_4 and produced a Ag-doped HAp layer (Figures 2(c) and 2(d)).

The EDS elemental map of the disk coated by Ag-doped HAp (Figure 5(a)) shows evenly distribution Ag supporting the lack of compact accumulation of Ag. Ca and P were also evenly distributed supporting the presence of HAp. The trace level of F is a contaminant from the electrochemical

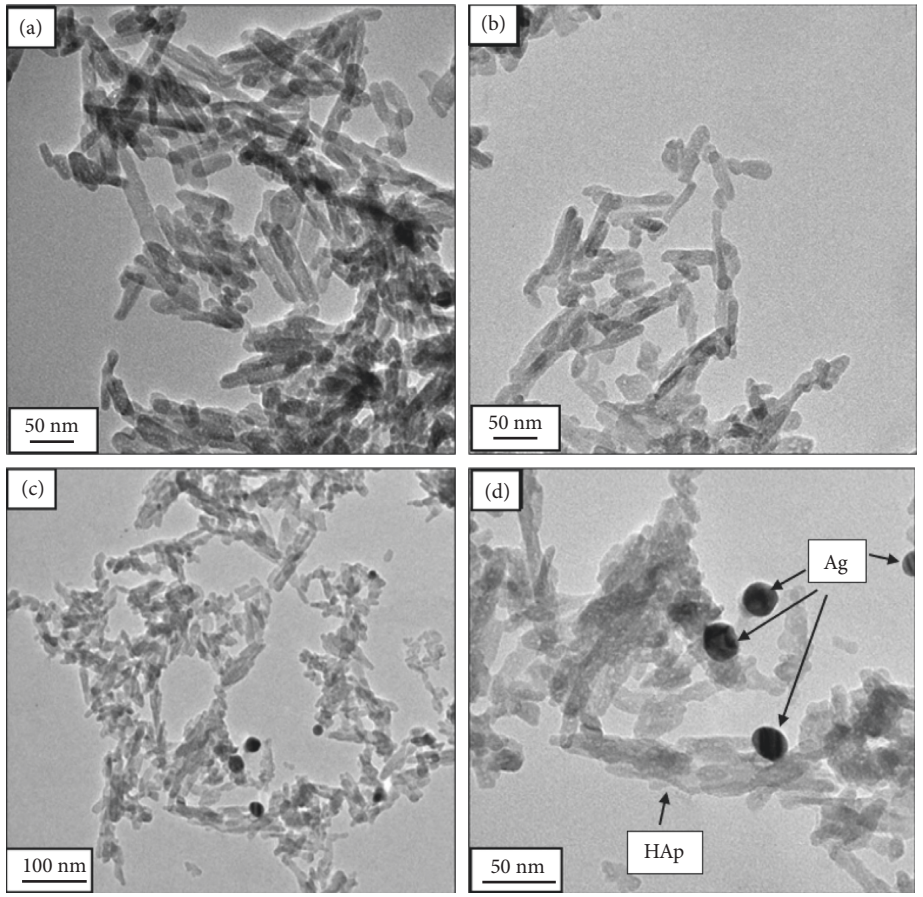

Figure 7: TEM micrographs of sonosynthesized HAp (a, b) and Ag-HAp (c, d).

anodization process. Figure 5(b) represents an EDS line scan of the same region as in Figure 5(a) that also quantitatively characterizes the element abundance on the surface. Table 2 represents the elemental weight percentage of surface materials obtained using the layered mapping and line scan EDS. This provides another evidence of evenly distributed Ag (0.3% on both) and HAp elements (Ca of 1.9% and 2.1%; P of 1.3% and 1.4%) using the sonosynthetic method.

To access the effect of the TiO_2 NT disk on the coprecipitation of Ag_3PO_4 and HAp, the precipitates formed in the presence of the TiO_2 NT disk were isolated and characterized. The supernatant aqueous suspension was drop cast on a TEM grid for EDS analysis to investigate the distribution of Ag in the particulate (Figure 6(a)). The elemental maps of Ag and Ca (Figures 6(b)–6(e)) show the particles, where both elements can be found simultaneously, which suggests either an incorporation of Ag to the HAp phase, or a fine mixture of calcium and silver phosphates.

3.3. TEM Analysis of Ag-Free and Ag-Doped HAp. Figure 7 shows TEM images of the supernatant material obtained through coprecipitation of Ag_3PO_4 and HAp in the presence of TiO_2 NT disks. The rod-like (HAp) and spherical (Ag_3PO_4) morphology of the nanocrystals are characteristic of HAp and Ag_3PO_4. In fact, neither the morphology nor the size of the HAp crystals was affected by the Ag_3PO_4 coprecipitation technique. This implies that the physical and chemical properties of HAp are unlikely to be affected by their coprecipitation and, therefore, should be retained for further applications.

4. Conclusions

A highly uniform distribution of Ag over the surface of a TiO_2 NT disk was achieved by the deposition of Ag_3PO_4 crystals followed by photolysis. Coprecipitation of Ag_3PO_4 and HAp on a TiO_2 NT disk surface leads to an even distribution of Ag over the surface as well. The availability of evenly distributed Ag and HAp codeposits creates an opportunity for the spatially controlled deposition and environment-controlled release of antibacterial Ag where it is most needed for bacterial infection while maintaining good adhesion of HAp to the TiO_2 surface for potential osteoblast adhesion and bone regeneration.

Data Availability

The data used to support the findings of this study are included within the article and can also be provided by the corresponding author upon request.

Conflicts of Interest

The authors declare that they have no conflicts of interest.

Acknowledgments

The authors thank the South Dakota Surface Engineering Research Center (SERC), NSF-MRI Grant CHE-1337707 for funding for the SEM instrument, NSF-CRIF:MU Grant CHE-0840507 for funding for the TEM instrument, the Materials Science Ph.D. Program of the State of South Dakota, and the USD Department of Chemistry. The authors also thank Brandon Karels for help with TEM imaging.

References

[1] M. Geetha, A. K. Singh, R. Asokamani, and A. K. Gogia, "Ti based biomaterials, the ultimate choice for orthopaedic implants—a review," *Progress in Materials Science*, vol. 54, no. 3, pp. 397–425, 2009.

[2] K. S. Brammer, S. Oh, C. J. Cobb, L. M. Bjursten, H. van der Heyde, and S. Jin, "Improved bone-forming functionality on diameter-controlled TiO_2 nanotube surface," *Acta Biomaterialia*, vol. 5, no. 8, pp. 3215–3223, 2009.

[3] S. B. Goodman, Z. Yao, M. Keeney, and F. Yang, "The future of biologic coatings for orthopaedic implants," *Biomaterials*, vol. 34, no. 13, pp. 3174–3183, 2013.

[4] C. Castellani, R. A. Lindtner, P. Hausbrandt et al., "Bone-implant interface strength and osseointegration: biodegradable magnesium alloy versus standard titanium control," *Acta Biomaterialia*, vol. 7, no. 1, pp. 432–440, 2011.

[5] S. A. Jovanovic, H. Spiekermann, and E. J. Richter, "Bone regeneration around titanium dental implants in dehisced defect sites: a clinical study," *International Journal of Oral and Maxillofacial Implants*, vol. 7, no. 2, pp. 233–245, 1992.

[6] E. Anitua, G. Orive, R. Pla, P. Roman, V. Serrano, and I. Andía, "The effects of PRGF on bone regeneration and on titanium implant osseointegration in goats: a histologic and histomorphometric study," *Journal of Biomedical Materials Research Part A*, vol. 91, no. 1, pp. 158–165, 2009.

[7] S. Oh, R. Finones, C. Daraio, L. Chen, and S. Jin, "Growth of nano-scale hydroxyapatite using chemically treated titanium oxide nanotubes," *Biomaterials*, vol. 26, no. 24, pp. 4938–4943, 2005.

[8] K. Rashwan and G. Sereda, "Applications of nanoparticles through surface functionalization," in *ACS Symposium Series*, pp. 91–105, vol. 1224American Chemical Society, Washington, DC, USA, 2016.

[9] G. Sereda, K. Rashwan, B. Karels, and A. Fritza, "Materials science versus tooth hypersensitivity," in *Dekker Encyclopedia of Nanoscience and Nanotechnology*, pp. 1–6, CRC Press, Boca Raton, FL, USA, 3rd edition, 2014.

[10] P. Ducheyne, W. Van Raemdonck, J. C. Heughebaert, and M. Heughebaert, "Structural analysis of hydroxyapatite coatings on titanium," *Biomaterials*, vol. 7, no. 2, pp. 97–103, 1986.

[11] D. R. Cooley, A. F. Van Dellen, J. O. Burgess, and A. S. Windeler, "The advantages of coated titanium implants prepared by radiofrequency sputtering from hydroxyapatite," *Journal of Prosthetic Dentistry*, vol. 67, no. 1, pp. 93–100, 1992.

[12] M. C. De Andrade, M. S. Sader, M. R. T. Filgueiras, and T. Ogasawara, "Microstructure of ceramic coating on titanium surface as a result of hydrothermal treatment," *Journal of Materials Science: Materials in Medicine*, vol. 11, no. 11, pp. 751–755, 2000.

[13] D. A. Puleo, L. A. Holleran, R. H. Doremus, and R. Bizios, "Osteoblast responses to orthopedic implant materialsin vitro," *Journal of Biomedical Materials Research*, vol. 25, no. 6, pp. 711–723, 1991.

[14] O. Salata, "Applications of nanoparticles in biology and medicine," *Journal of Nanobiotechnology*, vol. 2, p. 3, 2004.

[15] A. Satsangi, N. Satsangi, R. Glover, R. K. Satsangi, and J. L. Ong, "Osteoblast response to phospholipid modified titanium surface," *Biomaterials*, vol. 24, no. 25, pp. 4585–4589, 2003.

[16] L. Zhao, H. Wang, K. Huo et al., "Antibacterial nanostructured titania coating incorporated with silver nanoparticles," *Biomaterials*, vol. 32, no. 24, pp. 5706–5716, 2011.

[17] T. J. Webster and J. U. Ejiofor, "Increased osteoblast adhesion on nanophase metals: Ti, Ti_6Al_4V, and CoCrMo," *Biomaterials*, vol. 25, no. 19, pp. 4731–4739, 2004.

[18] G. Mendonça, D. B. S. Mendonça, F. J. L. Aragão, and L. F. Cooper, "Advancing dental implant surface technology-from micron to nanotopography," *Biomaterials*, vol. 29, no. 28, pp. 3822–3835, 2008.

[19] C. S. Hajicharalambous, J. Lichter, W. T. Hix, M. Swierczewska, M. F. Rubner, and P. Rajagopalan, "Nano- and sub-micron porous polyelectrolyte multilayer assemblies: biomimetic surfaces for human corneal epithelial cells," *Biomaterials*, vol. 30, no. 23-24, pp. 4029–4036, 2009.

[20] L. Zhao, S. Mei, W. Wang, P. K. Chu, Z. Wu, and Y. Zhang, "The role of sterilization in the cytocompatibility of titania nanotubes," *Biomaterials*, vol. 31, no. 8, pp. 2055–2063, 2010.

[21] L. Zhao, S. Mei, P. K. Chu, Y. Zhang, and Z. Wu, "The influence of hierarchical hybrid micro/nano-textured titanium surface with titania nanotubes on osteoblast functions," *Biomaterials*, vol. 31, no. 19, pp. 5072–5082, 2010.

[22] S. Oh, C. Daraio, L.-H. Chen, T. R. Pisanic, R. R. Fiñones, and S. Jin, "Significantly accelerated osteoblast cell growth on aligned TiO_2 nanotubes," *Journal of Biomedical Materials Research Part A*, vol. 78, no. 1, pp. 97–103, 2006.

[23] S. Imade, R. Mori, Y. Uchio, and S. Furuya, "Effect of implant surface roughness on bone fixation: the differences between bone and metal pegs," *Journal of Orthopaedic Science*, vol. 14, no. 5, pp. 652–657, 2009.

[24] R. Lange, F. Lüthen, U. Beck, J. Rychly, A. Baumann, and B. Nebe, "Cell-extracellular matrix interaction and physicochemical characteristics of titanium surfaces depend on the roughness of the material," *Biomolecular Engineering*, vol. 19, no. 2, pp. 255–261, 2002.

[25] G. Crawford, N. Chawla, K. Das, S. Bose, and A. Bandyopadhyay, "Microstructure and deformation behavior of biocompatible TiO2 nanotubes on titanium substrate☆," *Acta Biomaterialia*, vol. 3, no. 3, pp. 359–367, 2007.

[26] K. C. Popat, M. Eltgroth, T. J. LaTempa, C. A. Grimes, and T. A. Desai, "Decreased *Staphylococcus epidermis* adhesion and increased osteoblast functionality on antibiotic-loaded titania nanotubes," *Biomaterials*, vol. 28, no. 32, pp. 4880–4888, 2007.

[27] K. Das, S. Bose, and A. Bandyopadhyay, "TiO2nanotubes on Ti: influence of nanoscale morphology on bone cell-materials interaction," *Journal of Biomedical Materials Research Part A*, vol. 90, no. 1, pp. 225–237, 2009.

[28] F. J. Gil, A. Padrós, J. M. Manero, C. Aparicio, M. Nilsson, and J. A. Planell, "Growth of bioactive surfaces on titanium and its alloys for orthopaedic and dental implants," *Materials Science and Engineering: C*, vol. 22, no. 1, pp. 53–60, 2002.

[29] L. Le Guéhennec, A. Soueidan, P. Layrolle, and Y. Amouriq, "Surface treatments of titanium dental implants for rapid osseointegration," *Dental Materials*, vol. 23, no. 7, pp. 844–854, 2007.

[30] K. G. Neoh, X. Hu, D. Zheng, and E. T. Kang, "Balancing osteoblast functions and bacterial adhesion on functionalized titanium surfaces," *Biomaterials*, vol. 33, no. 10, pp. 2813–2822, 2012.

[31] P. DeVasConCellos, S. Bose, H. Beyenal, A. Bandyopadhyay, and L. G. Zirkle, "Antimicrobial particulate silver coatings on stainless steel implants for fracture management," *Materials Science and Engineering: C*, vol. 32, no. 5, pp. 1112–1120, 2012.

[32] N. J. Shah, M. N. Hyder, J. S. Moskowitz et al., "Surface-mediated bone tissue morphogenesis from tunable nano-layered implant coatings," *Science Translational Medicine*, vol. 5, no. 191, p. 191, 2013.

[33] S. Svensson, F. Suska, L. Emanuelsson et al., "Osseointegration of titanium with an antimicrobial nanostructured noble metal coating," *Nanomedicine: Nanotechnology, Biology and Medicine*, vol. 9, no. 7, pp. 1048–1056, 2013.

[34] L. Gaviria, J. P. Salcido, T. Guda, and J. L. Ong, "Current trends in dental implants," *Journal of Korean Association of Oral and Maxillofacial Surgeons*, vol. 40, no. 2, pp. 50–60, 2014.

[35] B. L. Foss, N. Ghimire, R. Tang, Y. Sun, and Y. Deng, "Bacteria and osteoblast adhesion to chitosan immobilized titanium surface: a race for the surface," *Colloids and Surfaces B: Biointerfaces*, vol. 134, pp. 370–376, 2015.

[36] H.-S. Kim, Y.-J. Kim, J.-H. Jang, and J.-W. Park, "Surface engineering of nanostructured titanium implants with bioactive ions," *Journal of Dental Research*, vol. 95, no. 5, pp. 558–565, 2016.

[37] C. Caparros, M. Ortiz-Hernandez, M. Molmeneu et al., "Bioactive macroporous titanium implants highly interconnected," *Journal of Materials Science: Materials in Medicine*, vol. 27, no. 10, p. 151, 2016.

[38] P. J. Govindharajulu, X. Chen, Y. Li, C. J. Rodriguez-Cabello, M. Battacharya, and C. Aparicio, "Chitosan-recombinamer layer-by-layer coatings for multifunctional implants," *International Journal of Molecular Sciences*, vol. 18, no. 2, p. 369, 2017.

[39] A. Besinis, S. D. Hadi, H. R. Le, C. Tredwin, and R. D. Handy, "Antibacterial activity and biofilm inhibition by surface modified titanium alloy medical implants following application of silver, titanium dioxide and hydroxyapatite nanocoatings," *Nanotoxicology*, vol. 11, no. 3, pp. 1–12, 2017.

[40] T. Wang, Z. Weng, X. Liu, K. W. K. Yeung, H. Pan, and S. Wu, "Controlled release and biocompatibility of polymer/titania nanotube array system on titanium implants," *Bioactive Materials*, vol. 2, no. 1, pp. 44–50, 2017.

[41] Y. Huang, Z. Xu, X. Zhang et al., "Nanotube-formed Ti substrates coated with silicate/silver co-doped hydroxyapatite as prospective materials for bone implants," *Journal of Alloys and Compounds*, vol. 697, pp. 182–199, 2017.

[42] V. Alt, "Antimicrobial coated implants in trauma and orthopaedics—a clinical review and risk-benefit analysis," *Injury*, vol. 48, no. 3, pp. 599–607, 2017.

[43] G. Crawford and N. Chawla, "Porous hierarchical TiO2 nanostructures: processing and microstructure relationships," *Acta Materialia*, vol. 57, no. 3, pp. 854–867, 2009.

[44] Z. Guo, C. Chen, Q. Gao, Y. Li, and L. Zhang, "Fabrication of silver-incorporated TiO_2 nanotubes and evaluation on its antibacterial activity," *Materials Letters*, vol. 137, pp. 464–467, 2014.

[45] A. Gao, R. Hang, X. Huang et al., "The effects of titania nanotubes with embedded silver oxide nanoparticles on bacteria and osteoblasts," *Biomaterials*, vol. 35, no. 13, pp. 4223–4235, 2014.

[46] S. Mei, H. Wang, W. Wang et al., "Antibacterial effects and biocompatibility of titanium surfaces with graded silver incorporation in titania nanotubes," *Biomaterials*, vol. 35, no. 14, pp. 4255–4265, 2014.

[47] Y. Xie and Y. Meng, "SERS performance of graphene oxide decorated silver nanoparticle/titania nanotube array," *RSC Advances*, vol. 4, no. 79, pp. 41734–41743, 2014.

[48] A. Agarwal, T. L. Weis, M. J. Schurr et al., "Surfaces modified with nanometer-thick silver-impregnated polymeric films that kill bacteria but support growth of mammalian cells," *Biomaterials*, vol. 31, no. 4, pp. 680–690, 2010.

[49] I. Sondi and B. Salopek-Sondi, "Silver nanoparticles as antimicrobial agent: a case study on *E. coli* as aBmodel for Gram-negative bacteria," *Journal of Colloid and Interface Science*, vol. 275, no. 1, pp. 177–182, 2004.

[50] L. Zhao, P. K. Chu, Y. Zhang, and Z. Wu, "Antibacterial coatings on titanium implants," *Journal of Biomedical Materials Research Part B: Applied Biomaterials*, vol. 91, no. 1, pp. 470–480, 2009.

[51] J. Hardes, H. Ahrens, C. Gebert et al., "Lack of toxicological side-effects in silver-coated megaprostheses in humans," *Biomaterials*, vol. 28, no. 18, pp. 2869–2875, 2007.

[52] V. Alt, T. Bechert, P. Steinrücke et al., "An in vitro assessment of the antibacterial properties and cytotoxicity of nanoparticulate silver bone cement," *Biomaterials*, vol. 25, no. 18, pp. 4383–4391, 2004.

[53] B. S. Necula, L. E. Fratila-Apachitei, S. A. J. Zaat, I. Apachitei, and J. Duszczyk, "In vitro antibacterial activity of porous TiO_2-Ag composite layers against methicillin-resistant *Staphylococcus aureus*," *Acta Biomaterialia*, vol. 5, no. 9, pp. 3573–3580, 2009.

[54] M. Niraula, S. Adhikari, D. Y. Lee et al., "Titania nanotube-silver phosphate hybrid heterostructure for improved visible light induced photocatalysis," *Chemical Physics Letters*, vol. 593, pp. 193–197, 2014.

[55] R. Liu, P. Hu, and S. Chen, "Photocatalytic activity of Ag_3PO_4 nanoparticle/TiO_2 nanobelt heterostructures," *Applied Surface Science*, vol. 258, no. 24, pp. 9805–9809, 2012.

[56] V. Uskoković, S. S. Batarni, J. Schweicher, A. King, and T. A. Desai, "Effect of calcium phosphate particle shape and size on their antibacterial and osteogenic activity in the delivery of antibiotics in vitro," *ACS Applied Materials and Interfaces*, vol. 5, no. 7, pp. 2422–2431, 2013.

[57] A. Dubnika, D. Loca, V. Rudovica, M. B. Parekh, and L. Berzina-Cimdina, "Functionalized silver doped hydroxyapatite scaffolds for controlled simultaneous silver ion and drug delivery," *Ceramics International*, vol. 43, no. 4, pp. 3698–3705, 2017.

[58] M. Ribeiro, F. J. Monteiro, and M. P. Ferraz, "Infection of orthopedic implants with emphasis on bacterial adhesion process and techniques used in studying bacterial-material interactions," *Biomatter*, vol. 2, no. 4, pp. 176–194, 2014.